



Nonlinear vibration and postbuckling analysis of a single layer graphene sheet embedded in a polymer matrix

M.H. Mahdavi, L.Y. Jiang*, X. Sun

Department of Mechanical and Materials Engineering, The University of Western Ontario, London, Ontario N6A 5B9, Canada

HIGHLIGHTS

- ▶ Consider nonlinear interfacial vdW forces on embedded GS based on cohesive law.
- ▶ Implement harmonic balance method to solve the nonlinear problem.
- ▶ Derive explicit expressions for nonlinear frequencies and postbuckling loads of GS.
- ▶ Investigate the effects of aspect ratio, mode number, and in-plane loads.
- ▶ Demonstrate the significance of considering nonlinearity of vdW forces for embedded GS.

ARTICLE INFO

Article history:

Received 3 April 2012
 Received in revised form
 25 April 2012
 Accepted 27 April 2012
 Available online 5 May 2012

ABSTRACT

Nonlinear vibration and postbuckling behavior of a single layer graphene sheet (SLGS) embedded in a polymer matrix aroused by the nonlinear van der Waals (vdW) forces are investigated using the Kirchhoff plate theory. The interfacial vdW forces are described by a nonlinear function in terms of the graphene deflection. Through harmonic balance method, the nonlinear relation between deflection amplitudes and resonant frequencies of free vibrations of the SLGS and its postbuckling equilibrium path are derived. It is found that variation of resonant frequencies of an embedded SLGS is less dependent on the graphene aspect ratio and mode numbers as compared with a free-standing one. In-plane load effects upon the vibrational behavior of the SLGS and its postbuckling are also discussed. Simulation results have demonstrated the significance of considering the surrounding medium effect and its nonlinearity in the study of the vibration and buckling of the embedded graphene with applications in nanocomposites.

© 2012 Elsevier B.V. All rights reserved.

1. Introduction

Up to now, different allotropes of carbon, ranging from diamond and graphite (3D), to graphene (2D) [1], to nanotubes (1D) [2], and to fullerenes (0D) [3], have been reported and attracted tremendous attention from research communities to explore their properties. Among these novel materials, the discovery of graphene [1] is considered as a breakthrough in the nanotechnology era due to its extraordinary mechanical, electrical and thermal properties [4–6]. These superior properties have foreseen the potential applications of graphene in nanocomposites and as a revolutionary substitute of silicon in electronics. When graphene is incorporated into polymer matrices, the properties of host materials manifest remarkable improvement [7,8], for example, the mechanical and thermal properties of these materials rank

among the best in comparison with other carbon-based composites [8]. Emerging as a new class of materials, these graphene-based composites may hold promise for many applications, such as photocatalysis [9], lithium-ion batteries, fuel cells, and sensors [10], electronics [11], transparent conductors [12], and supercapacitors [13].

To make the full potential applications of graphene-based polymer composites, it is essential to understand their mechanical behavior, which has become a hot topic recently. Due to extreme difficulties in conducting experiments on nanoscale materials and computing expensiveness of atomistic studies, many researchers have pursued continuum mechanics models for the analysis of graphene. In particular, considerable efforts have been devoted to understanding vibrational and buckling behavior of graphene or graphene-based composites. The vibrational behavior of multi-layer graphene sheets (MLGSs) embedded in a polymer medium was investigated by considering the vdW forces from both adjacent layers [14,15] and surrounding medium [16,17]. Wang and He [18] studied the effect of initial stress on the vibration of MLGSs with the

* Corresponding author. Tel.: +1 519 661 2111x80422; fax: +1 519 661 3020.
 E-mail address: lyjiang@eng.uwo.ca (L.Y. Jiang).

consideration of interlayer vdW forces. The influence of boundary conditions on the vibration of the embedded MLGSs was studied in Ref. [19]. Pradhan and Kumar conducted the vibration analysis of a single layer graphene sheet (SLGS) embedded in an elastic medium considering orthotropic properties of graphene [20]. In order to incorporate the small scale effects, the nonlocal elasticity theory has also been adopted by some researchers to study the vibrational and buckling behavior of graphene or graphene-based composites [19–28]. It has been reported that the nonlocal plate model is necessary in vibration analysis of graphene sheets with a length less than 8 nm [21]. It is expected that with the increase of the graphene size, the nonlocal effect becomes less. For example, the fundamental resonant frequencies calculated by the local plate theory and nonlocal plate theory are very close when the plate side size equals to 10 nm as shown in Fig. 2 of Ref. [21]. Among these studies, the higher order shear deformation plate theory in which the displacement field is expanded up to the third-order of the thickness coordinate was used by Pradhan and coworker [24,25] to get more accurate prediction on the vibrational and buckling behavior of a graphene sheet.

It should be mentioned that most existing continuum studies of graphene are linear analyses. Until recently, there have been several investigations on the matter of different aspects of nonlinearities for carbon nanotubes (CNT) and graphene. Regarding CNTs, the nonlinearity due to large deformation [29–31], interlayer nonlinear vdW interactions between adjacent tubes [32,33], and nonlinear interfacial vdW forces from surrounding medium [33,34] has been accounted in studying the vibrational and buckling behavior of CNT or CNT-based composites. In addition, there are also a few numbers of nonlinear studies on graphene. For example, Sadeghi and Naghdabadi [35] introduced a hybrid atomistic-structural element based on the empirical inter-atomic potential function for modeling the geometrical and material nonlinearity in dynamic response of a graphene sheet. Shen et al. [36] studied the nonlinear vibration behavior of a simply supported SLGS with geometric nonlinearity under different temperatures. In their work, the nonlocal parameter was obtained by matching the natural frequencies of graphene sheet obtained from the molecular dynamics simulation results with the numerical results obtained from the nonlocal plate model. Recently, Jomehzadeh and Saidi [37] studied large amplitude vibrations of MLGSs based on the von Karman plate model and the Eringen's nonlocal elasticity theory. The harmonic balance method was used to find the solutions of free nonlinear vibration for single, double, and triple layer graphene sheets with different boundary conditions. With the consideration of nonlinear vdW interaction between any two adjacent layers of MLGSs and large deformation of each individual layer, Wang et al. [38] developed a continuum mechanics model to analyze the vibration of MLGSs. The nonlinear amplitude–frequency relations of double layer graphene sheets (DLGSs) were derived in their study. Mianroodi et al. [39] introduced a membrane model which is capable of modeling the nonlinear vibration of SLGS by including the effects of stretching due to large deflection. In their work, the finite difference method was used to solve the nonlinear governing equation numerically with different boundary and initial conditions.

For the embedded graphene in polymer matrix, the surrounding medium was usually described by a Winkler model in most existing studies. In such a model, the surrounding medium was assumed to act as linear springs exerting pressure on the graphene sheet, which is linearly proportional to the deflection of the graphene. Different arbitrary values for the stiffness of spring could be assigned to represent the stiffness of the surrounding medium. In order to accurately account for the nanoscale interaction at the interface between graphene sheet and polymer medium, Behfar and Naghdabadi [16] calculated the exact value

for the stiffness of such a linear spring based on the vdW interaction forces. However, this interfacial vdW force governed by the Lenard-Jones potential is intrinsically nonlinear [40]. The effect of such nonlinear interfacial vdW forces from the surrounding medium on the vibrational behavior of a single-walled carbon nanotube (SWCNT) embedded in a polymer matrix was studied by Mahdavi et al. [34] using conventional beam theories. It was found that the nonlinear vdW forces from the surrounding medium had significant effect on the resonant frequencies of the embedded SWCNT. Hence, it is natural to believe that this nonlinear vdW force might play an important role on the vibrational and buckling behavior of the embedded graphene. To the authors' best knowledge, such an atomistic-based nonlinear interaction effect on the vibration and buckling of embedded graphene has not been studied thus far. Therefore, the objective of the current work is to investigate the nonlinear vibration and postbuckling of an embedded SLGS aroused by the nonlinear vdW interaction forces from the surrounding medium using classic plate theory. The effect of in-plane load on such nonlinear vibration and postbuckling behavior will also be examined. Simulation results will demonstrate the significance of considering the surrounding medium effect and its nonlinearity in the study of the vibration and buckling of the embedded graphene.

2. Problem formulation

The resonant frequencies and the buckling of the embedded SLGS will be studied by the classical Kirchhoff plate theory [41] in this work. Since the nonlinearity source is from the interfacial vdW forces, the nonlinear expression of the resultant pressure exerted by the surrounding polymer matrix to the graphene will be firstly derived from the interfacial cohesive law based on the vdW forces [40]. Using harmonic balance method, an explicit expression for the resonant frequencies of the nonlinear vibration of the embedded SLGS with simply supported boundary condition will be derived correspondingly.

2.1. Nonlinear expression of interfacial pressure from vdW interaction forces

In the absence of mechanical interlocking and covalent bonds at the graphene/polymer interface, the interfacial interaction between the graphene and the polymer comes from vdW forces. This interaction can be well described by the cohesive energy per unit area between a graphene and a polymer matrix as derived by Jiang et al. [40] based on the Lennard-Jones potential, i.e.,

$$\Phi(\delta) = \frac{2\pi}{3} \rho_p \rho_c \varepsilon \delta_0^3 \left[\frac{2}{15} \left(\frac{\delta_0}{\delta} \right)^9 - \left(\frac{\delta_0}{\delta} \right)^3 \right], \quad (1)$$

where δ is the interfacial spacing, ε and δ_0 are Lenard-Jones potential parameters, and ρ_p and ρ_c are volume density of polymer molecules and area density of carbon atoms on the graphene, respectively. The values of all these parameters vary with the interacting atoms or molecules. For example, if the polymer matrix is taken as polyethylene with the composition of repeating $-\text{CH}_2-$ units, these parameters are calculated as $\varepsilon = 0.004656$ eV, $\delta_0 = 0.3825$ nm, $\rho_p = 0.3052 \times 10^{29}$ molecules/m³ and $\rho_c = 3.8177 \times 10^{19}$ atom/m². The equilibrium interfacial spacing δ_e can be easily found from Eq. (1) as $\delta_e = (2/5)^{1/6} \delta_0$, and the interaction force per unit area exerted on the graphene surface is

derived as

$$P(\delta) = \frac{\partial \Phi}{\partial \delta} = 2\pi\rho_P\rho_C\varepsilon\delta_0^2 \left[\left(\frac{\delta_0}{\delta}\right)^4 - \frac{2}{5} \left(\frac{\delta_0}{\delta}\right)^{10} \right]. \quad (2)$$

Notice that the above equation is derived for a graphene resting on a polymer matrix, while in this study the graphene is embedded in a polymer matrix, the resultant pressure on the graphene layer is from both upper and lower matrices as shown in Fig. 1a. Therefore, this resultant pressure is an odd function of deviation of the graphene about the interfacial equilibrium distance δ_e , and its Taylor expansion can be expanded up to the third-order nonlinear terms as

$$p = -2 \left[P|_{\delta=\delta_e} + \frac{\partial P}{\partial \delta}|_{\delta=\delta_e} (\delta-\delta_e) + \frac{1}{6} \frac{\partial^3 P}{\partial \delta^3}|_{\delta=\delta_e} (\delta-\delta_e)^3 \right] = -\alpha_1 w - \alpha_3 w^3, \quad (3)$$

where $P|_{\delta=\delta_e} = 0$ and

$$\alpha_1 = 16\pi\rho_P\rho_C\varepsilon\delta_0 \left[\left(\frac{\delta_0}{\delta_e}\right)^{11} - \left(\frac{\delta_0}{\delta_e}\right)^5 \right],$$

$$\alpha_3 = \frac{16\pi\rho_P\rho_C\varepsilon}{\delta_0} \left[22 \left(\frac{\delta_0}{\delta_e}\right)^{13} - 5 \left(\frac{\delta_0}{\delta_e}\right)^7 \right], \quad (4)$$

which are the equivalent linear and nonlinear stiffness of the surrounding medium. The interfacial spacing change equals to the transverse deflection w of graphene, i.e., $\delta - \delta_e = w$.

2.2. Model development for equation of motion

For an isotropic SLGS with length a along x -axis, width b along y -axis and thickness h , as shown in Fig. 1b, in general case, it is subjected to biaxial compressive in-plane loads N_x and N_y on edges and distributed transverse load p per unit area due to the surrounding medium effect as given in Eq. (3). The governing equation for the vibration of a SLGS based on the Kirchhoff plate theory [41] can therefore be derived as

$$D\nabla^4 w + \alpha_1 w + \alpha_3 w^3 + \rho h \frac{\partial^2 w}{\partial t^2} + N_x \frac{\partial^2 w}{\partial x^2} + N_y \frac{\partial^2 w}{\partial y^2} = 0, \quad (5)$$

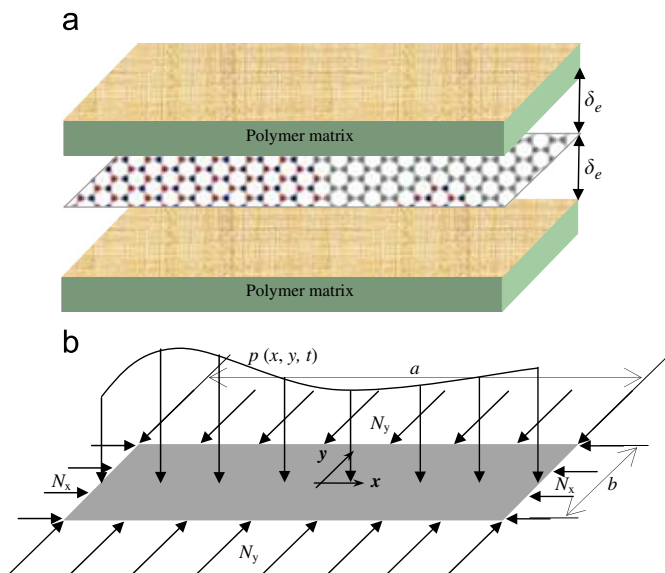


Fig. 1. (a) A single layer graphene sheet embedded in a polymeric matrix. In equilibrium state, the distance between the graphene sheet and the upper and lower matrix is δ_e , (b) schematic of a SLGS under in-plane loading N_x and N_y and interfacial pressure $p(x,y,t)$ from the surrounding medium.

where w is the transverse deflection of the sheet which is assumed to be positive in the upward direction, D is the bending stiffness of the plate defined as $Eh^3/12(1-\nu^2)$ with E and ν being Young's modulus and Poisson's ratio, ρ is the mass density and ∇^2 is the Laplace operator defined as

$$\nabla^2 = \frac{\partial^2}{\partial x^2} + \frac{\partial^2}{\partial y^2} \quad (6)$$

3. Solutions

It is known that exact analytical solutions are not available for the governing Eq. (5), therefore, approximate analytical solutions are pursued to characterize the vibration and postbuckling behavior of the embedded SLGS. By assuming harmonic solution $w(x,y,t) = AW(x,y)\sin\omega t$ with A and $W(x,y)$ representing the deflection amplitude and the vibration mode of the graphene, Eq. (5) can be rewritten as

$$D\nabla^4 W + \alpha_1 W + \alpha_3 A^2 W^3 \sin^2 \omega t - \rho h \omega^2 W + N_x \frac{\partial^2 W}{\partial x^2} + N_y \frac{\partial^2 W}{\partial y^2} = 0 \quad (7)$$

Eq. (7) reduces to the governing equation of a linear system simply by ignoring the nonlinear term α_3 . In the linear vibration analysis the deflection amplitude of the vibration is independent of frequency. However, the deflection amplitude in a nonlinear analysis is frequency-dependent and can be determined by different numerical or analytical approaches. In order to find the nonlinear resonant frequencies of the embedded SLGS, the harmonic balance method (HBM) [30,32–34,42] is employed, which is an approximate analytical approach for solving nonlinear oscillators generally with zero initial conditions. Following the same HBM procedure, Eq. (7) becomes

$$\gamma + \lambda_1 + \lambda_3 A^2 - \beta \omega^2 - N_x \eta_x - N_y \eta_y = 0, \quad (8)$$

in which

$$\gamma = D \left[\left(\frac{m\pi}{a}\right)^2 + \left(\frac{n\pi}{b}\right)^2 \right]^2 \int_{-(a/2)}^{a/2} \int_{-(b/2)}^{b/2} W^2(x,y) dy dx \times \int_0^{2\pi/\omega} \sin^2 \omega t dt, \quad (9a)$$

$$\lambda_1 = \alpha_1 \int_{-(a/2)}^{a/2} \int_{-(b/2)}^{b/2} W^2(x,y) dy dx \times \int_0^{2\pi/\omega} \sin^2 \omega t dt, \quad (9b)$$

$$\lambda_3 = \alpha_3 \int_{-(a/2)}^{a/2} \int_{-(b/2)}^{b/2} W^4(x,y) dy dx \times \int_0^{2\pi/\omega} \sin^4 \omega t dt, \quad (9c)$$

$$\beta = \rho h \int_{-(a/2)}^{a/2} \int_{-(b/2)}^{b/2} W^2(x,y) dy dx \times \int_0^{2\pi/\omega} \sin^2 \omega t dt, \quad (9d)$$

$$\eta_x = \left(\frac{m\pi}{a}\right)^2 \int_{-(a/2)}^{a/2} \int_{-(b/2)}^{b/2} W^2(x,y) dy dx \times \int_0^{2\pi/\omega} \sin^2 \omega t dt, \quad (9e)$$

$$\eta_y = \left(\frac{n\pi}{b}\right)^2 \int_{-(a/2)}^{a/2} \int_{-(b/2)}^{b/2} W^2(x,y) dy dx \times \int_0^{2\pi/\omega} \sin^2 \omega t dt \quad (9f)$$

Therefore, the relation between the resonant frequency and the deflection amplitude of an embedded SLGS subjected to in-plane load can be obtained from Eq. (8) if the vibration mode $W(x,y)$ is provided. In this study the SLGS is assumed to be simply supported on all edges, the corresponding vibration mode satisfying such boundary conditions is

$$W(x,y) = \sin \frac{m\pi x}{a} \sin \frac{n\pi y}{b} \quad (10)$$

Substituting this harmonic solution into Eq. (8) results in the corresponding deflection dependent nonlinear resonant frequency ω_{NL} as

$$\omega_{NL}^2 = \omega_L^2 + \frac{27}{64} \frac{1}{\rho h} \alpha_3 A^2 \tag{11}$$

in which ω_L is the linear resonant frequency represented by

$$\omega_L^2 = \frac{1}{\rho h} \left\{ D \left[\left(\frac{m\pi}{a} \right)^2 + \left(\frac{n\pi}{b} \right)^2 \right]^2 - N_x \left(\frac{m\pi}{a} \right)^2 - N_y \left(\frac{n\pi}{b} \right)^2 + \alpha_1 \right\} \tag{12}$$

Assuming no in-plane load, i.e., $N_x=N_y=0$, Eq. (12) is reduced to the same expression for the linear resonant frequency derived in Ref. [17], when transverse shear stress in their modeling is ignored. In addition, without surrounding medium effect by assuming $\alpha_1=0$, Eq. (12) can be simplified to the vibration of a free-standing SLGS as

$$\omega_{L, free}^2 = \frac{D}{\rho h} \left[\left(\frac{m\pi}{a} \right)^2 + \left(\frac{n\pi}{b} \right)^2 \right]^2 \tag{13}$$

which is the same as that of a simply supported SLGS obtained in Refs. [14,15].

In the buckling analysis of structures, it is interesting to obtain the postbuckling equilibrium path, which is defined as the relation between the applied loads and the deflection amplitudes [43] after the buckling load. Considering the compressive force acting on a column, the equivalent stiffness of the column will decrease with the increasing of the applied force and becomes zero when the force is close enough to its critical value [44]. Accordingly, the resonant frequency of the column becomes zero at this point. The same response is expected for plates. Therefore, the postbuckling equilibrium path of the embedded SLGS can be obtained by substituting $\omega=0$ into Eqs. (11) and (12) for the deflection-dependant postbuckling load and the critical buckling load, respectively. By letting $N_y=0$, the postbuckling load along x-axis N_x^{PB} is determined in terms of the deflection amplitude as

$$N_x^{PB} = N_x^B + \frac{27}{64} \left(\frac{a}{m\pi} \right)^2 \alpha_3 A^2, \tag{14}$$

in which N_x^B is the buckling load along x-axis,

$$N_x^B = \left(\frac{a}{m\pi} \right)^2 \left\{ D \left[\left(\frac{m\pi}{a} \right)^2 + \left(\frac{n\pi}{b} \right)^2 \right]^2 + \alpha_1 \right\} \tag{15}$$

When $N_x=0$, the postbuckling load along y-axis N_y^{PB} is derived as

$$N_y^{PB} = N_y^B + \frac{27}{64} \left(\frac{b}{n\pi} \right)^2 \alpha_3 A^2, \tag{16}$$

in which N_y^B is the buckling load along y-axis,

$$N_y^B = \left(\frac{b}{n\pi} \right)^2 \left\{ D \left[\left(\frac{m\pi}{a} \right)^2 + \left(\frac{n\pi}{b} \right)^2 \right]^2 + \alpha_1 \right\} \tag{17}$$

4. Numerical results and discussions

In order to investigate the effects of the interfacial vdW forces (α_1 and α_3) on the vibrational behavior of the embedded SLGS, the relationship between the deflection amplitude and the resonant frequency of the embedded SLGS with simply support (S-S) end boundary conditions will be presented. For a SLGS with S-S edges, the vibration mode is expressed as in Eq. (10). In numerical simulation, it is assumed that Young’s modulus, Poisson’s ratio, sheet thickness and mass density for the embedded SLGS are $E=1.02$ TPa, $h=0.34$ nm, $\nu=0.16$ and $\rho=2250$ kgm⁻³, respectively [14,15,20,38], and the surrounding medium of the graphene is taken as polyethylene. Accordingly, the deflection-dependent resonant frequencies can be determined using Eq. (11).

Without considering the in-plane load effect, Table 1 presents the linear resonant frequencies $f=\omega/2\pi$ of a free-standing (Eq. (13)) and an embedded SLGS ($\alpha_3=0$) with different aspect ratio a/b for different mode numbers. It is inferred from this table that the polymer matrix stiffness derived from the vdW interactions has a prominent effect on the resonant frequency of the embedded SLGS. For example, for a square SLGS with $a/b=1$, the linear resonant frequencies of the free-standing and the embedded SLGS corresponding to $m=n=1$ are 0.0665 THz and 1.3362 THz, respectively. However, this surrounding medium effect varies with the mode numbers and the aspect ratio of the graphene, i.e., the influence of the surrounding medium decreases with the increase of mode numbers m and n . It is also found that the resonant frequencies of both the free-standing and embedded graphenes at any mode shape numbers m and n decrease with the increase of aspect ratio a/b . The decrease rate is more pronounced for the free-standing SLGS in comparison with the embedded one, for example, with the increase of a/b from 1 to 10, the resonant frequency according to $m=n=1$ decreases about 1.98 times from 0.0665 THz to 0.0336 THz for the free-standing SLGS and about 1.0009 times from 1.3362 THz to 1.3350 THz for the embedded one. Moreover, for any given value of a/b , the increase of the resonant frequency with the mode shape numbers m and n is more noticeable for a free-standing SLGS. Therefore, it can be concluded from these data that the existence of the surrounding polymer medium may significantly influence the vibrational behavior of the embedded SLGS, which needs further investigation.

Table 1
Linear resonant frequencies $f_L=(\omega_L/2\pi)$ (THz) of a free-standing and an embedded graphene with S-S edges ($b=10$ nm).

	a/b	$m=1$			$m=2$			$m=3$		
		$n=1$	$n=2$	$n=3$	$n=1$	$n=2$	$n=3$	$n=1$	$n=2$	$n=3$
Embedded	1	1.3362	1.3449	1.3754	1.3449	1.3608	1.4029	1.3754	1.4029	1.4627
	2	1.3352	1.3421	1.3696	1.3362	1.3449	1.3754	1.3390	1.3507	1.3860
	3	1.3351	1.3416	1.3686	1.3355	1.3428	1.3710	1.3362	1.3449	1.3754
	4	1.3351	1.3414	1.3682	1.3352	1.3421	1.3696	1.3356	1.3432	1.3720
	5	1.3350	1.3413	1.3680	1.3351	1.3417	1.3689	1.3354	1.3424	1.3704
	10	1.3350	1.3412	1.3678	1.3350	1.3413	1.3680	1.3351	1.3415	1.3684
Free-standing	1	0.0665	0.1663	0.3325	0.1663	0.2660	0.4323	0.3325	0.4323	0.5986
	2	0.0416	0.1413	0.3076	0.0665	0.1663	0.3325	0.1081	0.2078	0.3741
	3	0.0369	0.1367	0.3030	0.0480	0.1478	0.3141	0.0665	0.1663	0.3325
	4	0.0353	0.1351	0.3014	0.0416	0.1413	0.3076	0.0520	0.1517	0.3180
	5	0.0346	0.1343	0.3006	0.0386	0.1383	0.3046	0.0452	0.1450	0.3113
	10	0.0336	0.1333	0.2996	0.0346	0.1343	0.3006	0.0362	0.1360	0.3023

Unlike the linear vibration, the resonant frequencies of the embedded SLGS due to the nonlinear vdW forces are deflection dependent. Fig. 2 shows the variation of the deflection amplitude of the embedded SLGS with the resonant frequencies for different aspect ratio a/b when mode numbers $m=n=1$. When the deflection amplitude is zero, the corresponding resonant frequencies are aroused by the linear part of the vdW interaction forces. It is clear that the nonlinear resonant frequency increases with the increase of the SLGS deflection amplitude for any given aspect ratio a/b , which exhibits a hardening nonlinearity. It is also indicated in this figure that the resonant frequencies of the embedded SLGS decrease with the increase of the aspect ratio a/b for any given deflection amplitude. However, when the SLGS aspect ratio is relatively big, for example $a/b > 5$, the aspect ratio effect upon the resonant frequencies is not significant. For different mode numbers m and n , Fig. 3 shows the variation of the deflection amplitude with the resonant frequency of an embedded SLGS with $a=b=10$ nm. As expected, the resonant frequency increases with the increase of the mode numbers. However, with the increase of the deflection amplitude, the

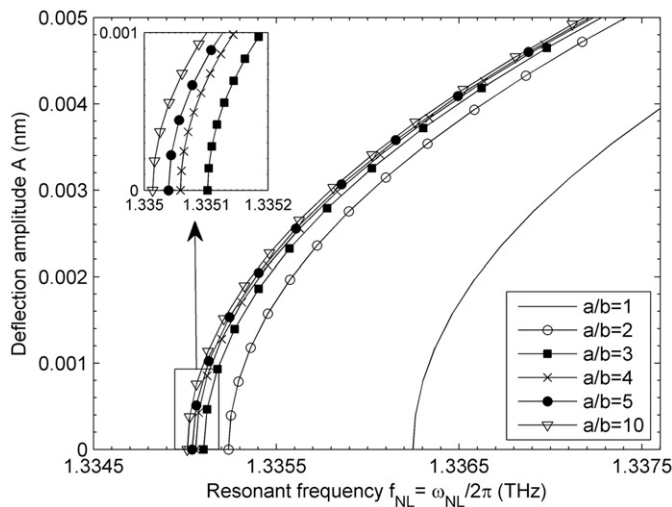


Fig. 2. Variation of the deflection amplitude with the resonant frequency of an embedded SLGS with S-S boundary conditions for different aspect ratio a/b ($m=n=1$ and $b=10$ nm).

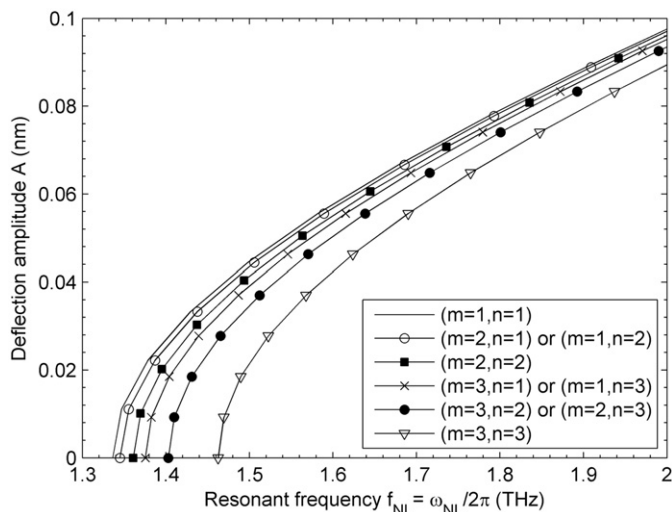


Fig. 3. Variation of the deflection amplitude with the resonant frequency of the embedded SLGS with S-S boundary conditions for different mode shapes numbers ($a=b=10$ nm).

dependence of the resonant frequency on the mode numbers becomes less for the nonlinear vibration. This result indicates that the nonlinear vibrational behavior could distinguish significantly from the linear vibrational behavior; therefore, it is essential to incorporate the nonlinear vdW interactions in predicting the mechanical properties of the embedded SLGS. In addition, it is also observed from this figure that at a given value of the nonlinear resonant frequency, the deflection amplitude for the lower mode shape is larger, which means that the system is softer at lower vibration modes.

The effect of in-plane loads on the vibrational behavior of a simply-supported SLGS embedded in the polymer matrix with $a=b=10$ nm for the first vibration mode ($m=n=1$) is presented in Figs. 4 and 5. The in-plane loads N_x and N_y are along the x -axis and the y -axis, respectively, and they are normalized by N_x^B and N_y^B , which are the buckling loads when a uni-axial load is applied either along the x -axis or the y -axis direction as indicated in Eqs. (15) and (17). Fig. 4 shows the effect of the uni-axial load (N_x for example) on the nonlinear resonant frequency of the embedded SLGS. As expected, the resonant frequency decreases with the compressive in-plane load while increases with the tensile one. For example, at a given resonant frequency, the deflection amplitude of the SLGS under compression is larger than the one under extension. It means that the system under compression load is softer than a system under extension. Particularly, when the in-plane load decreases gradually from a tensile load of $0.75N_x^B$ to zero and then to a compressive load of $0.75N_x^B$, the linear resonant frequency decreases from 1.7677 THz to 1.3362 THz and then to 0.6681 THz, respectively. It is concluded from this figure that the in-plane load effect is significant for the linear vibrational behavior of the embedded SLGS. However, with the increase of the deflection amplitude, the discrepancy among these curves becomes less which means that the nonlinear resonant frequency at larger deflection is less dependent on the in-plane load. Fig. 5 demonstrates the effect of the bi-axial in-plane load on the nonlinear resonant frequency of the SLGS. Similar trend to the results in Fig. 4 is observed. In particular, when the in-plane load decreases gradually from a tensile load of $0.75N_x^B$ to zero and then to a compressive load of $0.49N_x^B$, the linear resonant frequency decreases from 2.1128 THz to 1.3362 THz and then to 0.1890 THz. However, when the bi-axial loads N_x and N_y approach to half of their critical values, the linear resonant frequency approaches zero, which can be verified by substituting the half values of Eqs. (15) and (17) into Eq. (12).

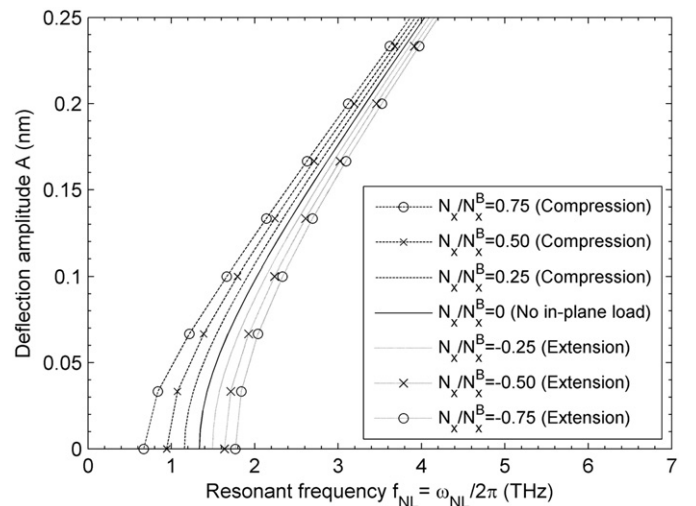


Fig. 4. Effect of uni-axial in-plane load N_x on the resonant frequency of an embedded SLGS with S-S boundary conditions ($m=n=1$ and $a=b=10$ nm).

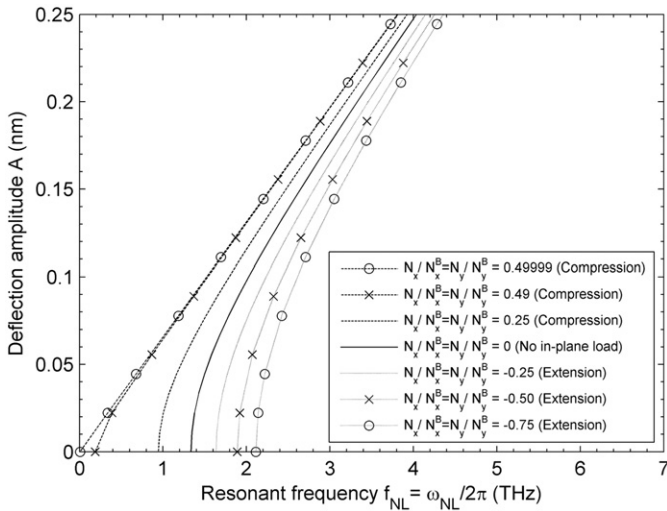


Fig. 5. Effect of bi-axial in-plane loads N_x and N_y on the resonant frequency of an embedded SLGS with S-S boundary conditions ($m=n=1$ and $a=b=10$ nm).

When the applied uni-axial in-plane load equals to the buckling load, the resonant frequency decreases to zero as derived in the formulation section. In what follows, the postbuckling behavior of the embedded SLGS due to the nonlinear vdW force from the surrounding medium will be examined. Fig. 6a and b demonstrate the postbuckling equilibrium paths for the embedded SLGS with S-S end conditions for different aspect ratios a/b ($b=10$ nm) when mode numbers $m=n=1$. In this figure, the postbuckling load is normalized by the buckling load for a square SLGS, i.e., $N_{y,a/b=1}^B$ and $N_{x,a/b=1}^B$ for Fig. 6a and b, respectively. It is found that this postbuckling load increases with the increase of the deflection amplitude and the aspect ratio has a significant effect upon this postbuckling equilibrium path. When N_x is set to zero, the postbuckling load decreases modestly with the increase of the aspect ratio a/b . Particularly, the values of the normalized buckling load corresponding to $a/b=1, 2, 3, 4$ and 5 are $1, 0.99849, 0.99829, 0.99822$ and 0.99819 , respectively. On the other hand, when N_y is set to zero, the postbuckling load increases dramatically with the increase of the aspect ratio a/b . For example, the values of normalized buckling load corresponding to $a/b=1, 2, 3, 4$ and 5 are $1, 3.9939, 8.9846, 15.9715$ and 24.9548 , respectively. Although this trend for both N_x and N_y is similar to what is expected for a free-standing graphene as long as a/b is higher than 1, the effect of the aspect ratio a/b on N_x is more pronounced than on N_y . This is attributed to the significant surrounding medium effect and indicates the necessity of considering the surrounding medium effect in the postbuckling analysis of the embedded SLGS.

Fig. 7 shows the postbuckling equilibrium paths of the embedded square SLGS ($a=b=10$ nm) with S-S end conditions for various buckling mode shapes when subjected to a uni-axial load N_x . In this figure, the postbuckling load N_x^{PB} is normalized with respect to $N_{x,m=n=1}^B$ which is the buckling load of a square SLGS when $m=n=1$. It is found that both the buckling and postbuckling loads increase with the increase of the mode number in the direction perpendicular to the applied load direction (i.e. n in this case), while the dependence of the buckling load on this mode number is not significant. However, an opposite trend is observed for the variation of both the buckling and postbuckling loads when the mode number along the applied load direction (i.e. m in this case) increases. Moreover, such dependence of the buckling load upon this mode number is much more prominent. For different mode numbers m and n , the normalized buckling loads ($N_x^B/N_{x,m=n=1}^B$) of the embedded square SLGS are

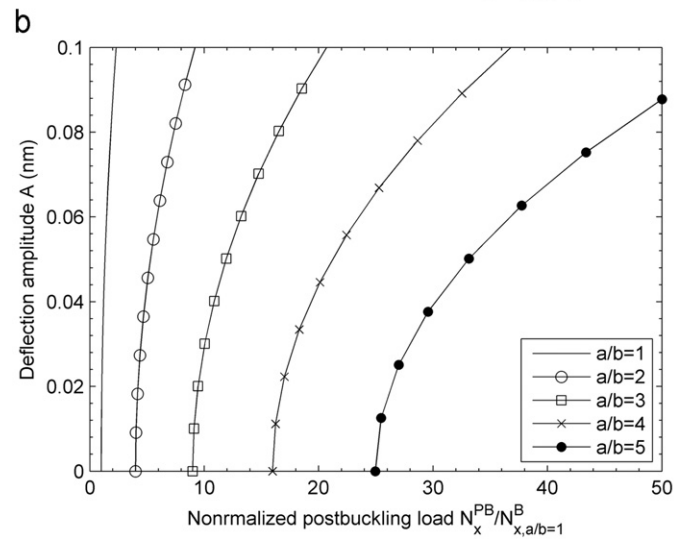
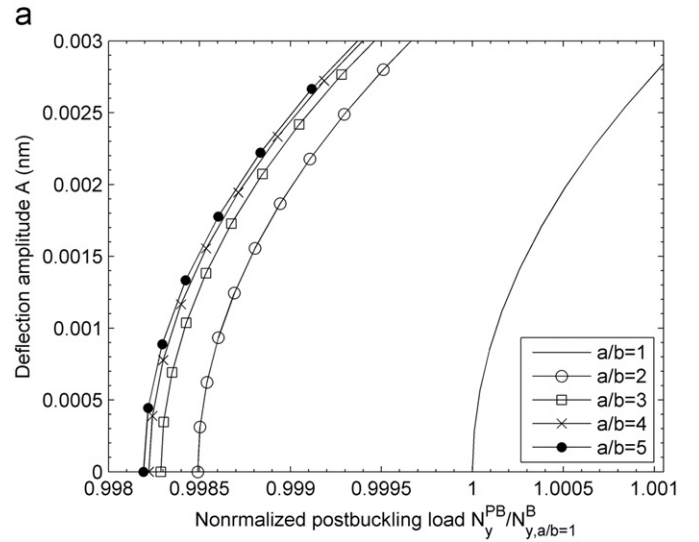


Fig. 6. Effect of aspect ratio a/b on the normalized postbuckling load of an embedded SLGS with S-S boundary conditions when subjected to a uni-axial load ($m=n=1$ and $b=10$ nm): (a) $N_x=0$ and $N_y \neq 0$, (b) $N_x \neq 0$ and $N_y=0$.

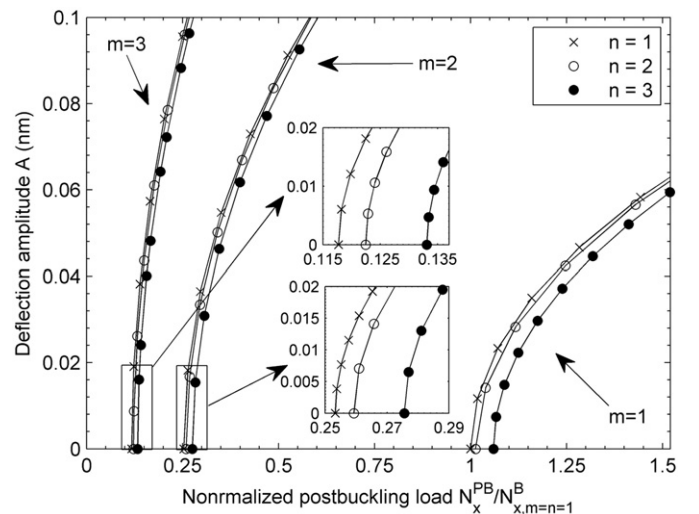


Fig. 7. Variation of the deflection amplitude with the normalized postbuckling load of an embedded SLGS with S-S boundary conditions for various modes of buckling ($a=b=10$ nm and $N_y=0$).

Table 2

The normalized uni-axial buckling load ($N_x^B/N_x^B, m=n=1, N_y=0$) of a free-standing and an embedded square SLGS with S-S boundary conditions for different mode numbers ($a=b=10$ nm).

	Embedded			Free-standing		
	$n=1$	$n=2$	$n=3$	$n=1$	$n=2$	$n=3$
$m=1$	1.0000	1.0130	1.0595	1.0000	6.2500	25.0000
$m=2$	0.2533	0.2593	0.2755	1.5625	4.0000	10.5625
$m=3$	0.1177	0.1225	0.1331	2.7778	4.6944	9.0000

listed in Table 2 for further comparison with the free-standing SLGS. For a free-standing SLGS, when the mode number perpendicular to the applied loading direction increases (i.e., n in this case), the buckling load increases, which is the same as what is observed for an embedded SLGS. Unlike the embedded graphene, the dependence of the buckling load on this mode number is very significant for the free-standing SLGS. However, when the mode number along the applied load direction increases (i.e., m in this case), the buckling load of a free-standing SLGS decreases as long as $m < n$, while increases when $m > n$. This discrepancy observed from the current study is believed to attribute to the substantial effect of the surrounding medium, i.e., the terms including α_1 and α_3 in Eqs. (14) and (16) are dominant. If the surrounding medium effect is not that big, i.e. α_1 and α_3 representing the linear and nonlinear interaction forces are small, the commonly accepted relation between the buckling loads and the mode numbers is expected to be the same as for a free-standing SLGS. With the consideration of the surrounding medium effect, it can also be concluded that the lowest buckling load for the uni-axial loading condition may not correspond to the first-order mode numbers (i.e., $m=n=1$), but corresponds to the lowest mode number perpendicular to the loading direction and decreases as long as the mode number along the loading direction increases depending on how big the exerted pressure is from the surrounding medium.

5. Conclusions

In summary, the nonlinear free vibration of an embedded single layer graphene sheet (SLGS) due to the nonlinear van der Waals interaction forces from its surrounding polymer matrix is studied through the classical Kirchhoff plate theory. Uni-axial and bi-axial in-plane load effect on the nonlinear vibration of an embedded SLGS and its postbuckling behavior are also investigated. The results show that the surrounding medium has a significant effect on the vibrational behavior of the embedded SLGS, which is quite different from that of the free-standing SLGS. The main results of the current work are summarized as follows:

1. Due to the nonlinear interaction forces, the resonant frequencies of the embedded SLGS are deflection-dependent and exhibit a hardening nonlinearity.
2. The dependence of the resonant frequencies of an embedded SLGS upon the graphene aspect ratio and mode numbers is less as compared with that for a free-standing SLGS due to the surrounding medium effect. When the SLGS aspect ratio is relatively big, for example $a/b > 5$, its effect upon the resonant frequencies is not significant.
3. The in-plane load and mode numbers have great effect upon the resonant frequencies of the embedded SLGS. However, with the increase of the deflection amplitude, such dependence of the nonlinear resonant frequencies on these factors becomes less.

4. The nonlinear van der Waals interaction forces arouse the dependence of the postbuckling load on the deflection amplitude. The postbuckling behavior of the embedded SLGS is also significantly affected by the SLGS aspect ratio and mode numbers. The critical buckling load prediction is quite different from that of a free-standing SLGS. For example, the critical buckling load of an embedded SLGS under uni-axial loading condition corresponds to the lowest mode number perpendicular to the loading direction and decreases as long as the mode number along the loading direction increases depending on how big the interaction pressures are exerted by the surrounding medium.

This analysis on the vibration and postbuckling behavior of the embedded SLGS is expected to be helpful for the design and application of graphene in nanocomposites.

Acknowledgment

This work is supported by the Natural Sciences and Engineering Research Council of Canada (NSERC) and Petro Canada Young Innovator Award.

References

- [1] A.K. Geim, K.S. Novoselov, Nature Materials 6 (2007) 183.
- [2] S. Iijima, Nature 354 (1991) 56.
- [3] H.W. Kroto, J.R. Heath, S.C. O'Brien, R.F. Curl, R.E. Smalley, Nature 318 (1985) 162.
- [4] C. Lee, X. Wei, J.W. Kysar, J. Hone, Science 321 (2008) 385.
- [5] A.H. Castro Neto, F. Guinea, N.M.R. Peres, K.S. Novoselov, A.K. Geim, Reviews of Modern Physics 81 (2009) 109.
- [6] A.A. Balandin, Nature Materials 10 (2011) 569.
- [7] S. Stankovich, D.A. Dikin, G.H.B. Dommett, K.M. Kohlhaas, E.J. Zimney, E.A. Stach, R.D. Piner, S.T. Nguyen, R.S. Ruoff, Nature 442 (2006) 282.
- [8] T. Ramanathan, A.A. Abdala, S. Stankovich, D.A. Dikin, M. Herrera-Alonso, R.D. Piner, D.H. Adamson, H.C. Schniepp, X. Chen, R.S. Ruoff, S.T. Nguyen, I.A. Aksay, R.K. Prud'Homme, L.C. Brinson, Nature Nanotechnology 3 (2008) 327.
- [9] H. Zhang, X. Lv, Y. Li, Y. Wang, J. Li, ACS Nano 4 (2010) 380.
- [10] X. Meng, D. Geng, J. Liu, R. Li, X. Sun, Nanotechnology 22 (2011) 165602.
- [11] G. Eda, M. Chhowalla, Nano Letters 9 (2009) 814.
- [12] S. Watcharotone, D.A. Dikin, S. Stankovich, R. Piner, I. Jung, G.H.B. Dommett, G. Evmenenko, S.E. Wu, S.F. Chen, C.P. Liu, S.B.T. Nguyen, R.S. Ruoff, Nano Letters 7 (2007) 1888.
- [13] Q. Wu, Y. Xu, Z. Yao, A. Liu, G. Shi, ACS Nano 4 (2010) 1963.
- [14] S. Kitipornchai, X.Q. He, K.M. Liew, Physical Review B 72 (2005) 075443.
- [15] X.Q. He, S. Kitipornchai, K.M. Liew, Nanotechnology 16 (2005) 2086.
- [16] K. Behfar, R. Naghdabadi, Composites Science and Technology 65 (2005) 1159.
- [17] K.M. Liew, X.Q. He, S. Kitipornchai, Acta Materialia 54 (2006) 4229.
- [18] L. Wang, X. He, Journal of Nanotechnology in Engineering and Medicine 1 (2010) 041004.
- [19] R. Ansari, B. Arash, H. Rouhi, Computational Materials Science 50 (2011) 3091.
- [20] S.C. Pradhan, A. Kumar, Composite Structures 93 (2011) 774.
- [21] B. Arash, Q. Wang, ASME Journal of Nanotechnology in Engineering and Medicine 2 (2011) 011012.
- [22] J.-X. Shi, Q.-Q. Ni, X.-W. Lei, T. Natsuki, Physica E (2012) <http://dx.doi.org/10.1016/j.physe.2011.12.023>.
- [23] T. Murmu, S.C. Pradhan, Journal of Applied Physics 105 (2009) 064319.
- [24] S.C. Pradhan, Physics Letters A 373 (2009) 4182.
- [25] S.C. Pradhan, B. Sahu, Journal of Computational and Theoretical Nanoscience 7 (2010) 1042.
- [26] S.C. Pradhan, T. Murmu, Physica E 42 (2010) 1293.
- [27] H. Babaei, A.R. Shahidi, Archive of Applied Mechanics 81 (2011) 1051.
- [28] S.H. Hashemi, A.T. Samaei, Physica E 43 (2011) 1400.
- [29] Y.M. Fu, J.W. Hong, X.Q. Wang, Journal of Sound and Vibration 296 (2006) 746.
- [30] Y. Yan, L.X. Zhang, W.Q. Wang, Journal of Applied Physics 103 (2008) 113523.
- [31] L.L. Ke, Y. Xiang, J. Yang, S. Kitipornchai, Computational Materials Science 47 (2009) 409.
- [32] K.Y. Xu, X.N. Guo, C.Q. Ru, Journal of Applied Physics 99 (2006) 064303.
- [33] M.M. Mahdavi, L.Y. Jiang, X. Sun, Physica E 43 (2011) 1813.
- [34] M.H. Mahdavi, L.Y. Jiang, X. Sun, Journal of Applied Physics 106 (2009) 114309.
- [35] M. Sadeghi, R. Naghdabadi, Nanotechnology 21 (2010) 105705.
- [36] L. Shen, H.S. Shen, C.L. Zhang, Computational Materials Science 48 (2010) 680.

- [37] E. Jomehzadeh, A.R. Saidi, Computational Materials Science 50 (2011) 1043.
- [38] J. Wang, X. He, S. Kitipornchai, H. Zhang, Journal of Physics D: Applied Physics 44 (2011) 135401.
- [39] J.R. Mianroodi, S.A. Niaki, R. Naghdabadi, M. Asghari, Nanotechnology 22 (2011) 305703.
- [40] L.Y. Jiang, Y. Huang, H. Jiang, G. Ravichandran, H. Gao, K.C. Hwang, B. Liu, Journal of the Mechanics and Physics of Solids 54 (2006) 2436.
- [41] S.S. Rao, Vibration of Continuous Systems, John Wiley and Sons, New Jersey, 2007.
- [42] Y.Z. Liu, L.Q. Chen, Nonlinear Vibration, High Education, Beijing, 2001 (in Chinese).
- [43] Z.C. Qiao, Applied Mathematics and Mechanics (English Edition) 14 (1993) 517.
- [44] C.L. Amba-Rao, Journal of the Acoustical Society of America 42 (1967) 900.